https://doi.org/10.48048/tis.2023.5496

Amorphous Cellulose: Graphene Oxide Composite Bead

Kongkiat Phuphantrakun[1], Achara Chandrachai[2] and Sanong Ekgasit[3,*]

[1]Technopreneurship and Innovation Management Program, Graduate School, Chulalongkorn University, Bangkok 10330, Thailand
[2]Chulalongkorn Business School, Chulalongkorn University, Bangkok 10330, Thailand
[3]Sensor Research Unit, Department of Chemistry, Faculty of Science, Chulalongkorn University, Bangkok 10330, Thailand

([*]Corresponding author's e-mail: sanong.e@chula.ac.th)

Received: 4 August 2022, Revised: 16 September 2022, Accepted: 23 September 2022, Published: 21 March 2023

Abstract

In this research, we developed an efficient method for the fabrication of amorphous cellulose-graphene oxide composite. Amorphous cellulose (AC) and amorphous cellulose-graphene oxide (ACGO) beads were fabricated via H_2SO_4 gelatinization using eucalyptus paper as a raw material. The cellulose gel was droplet-extruded into deionized (DI) water and transformed to a solid bead via the water-regeneration process. Small AC and ACGO quasi-sphere beads with diameter of 2 mm were obtained. The semicrystalline eucalyptus cellulose was transformed into amorphous cellulose after the regeneration process. The entrapment of graphene oxide (GO) by the amorphous cellulose was confirmed by scanning electron microscopy (SEM), fourier-transform infrared (FTIR) and raman spectroscopies (Raman). The gelatinization and regeneration processes offered a simple and efficient methodology for AC and ACGO bead fabrication.

Keywords: Cellulose dissolution, Amorphous cellulose, Cellulose gel, Cellulose-graphene oxide bead, Cellulose-graphene oxide composite

Introduction

Cellulose is an abundant natural material and a promising emerging "green material" because of its biocompatibility, biodegradability, and renewability [1-3]. Due to its unique properties, it is now considered as a viable component in various industries such as food packaging [4,5], pickering emulsifier [6], biodegradable film production [7,8], water purification [9,10], energy [11,12], security paper [13,14], and healthcare [15-17]. Its diverse applications increase future demand of cellulose market with a projected value of USD 783 million by 2025 [18].

Cellulose derivatives are categorized into various types such as cellulose nanofiber (CNF), nanocrystalline cellulose (CNC), cellulose acetate, bacteria cellulose (BC), amorphous cellulose (AC), and microcrystalline cellulose (MC) [2,19-21]. The derivatives are mainly produced from wood, cotton, pineapple leaf, abaca, sisal, flax, hemp and jute [22]. Wood is the most commercialized source of cellulose [23]. Among the woody plants, eucalyptus is an attractive material for cellulose production since it contained high portion of cellulose (up to 85.3 %) with low levels of hemicellulose and lignin [24]. For various cellulose derivatives, cellulose nanofibers, nanocrystalline cellulose, amorphous cellulose are the most common [9,10]. Interestingly, reports on AC composites are scarce despite its potential applications in many industries. AC synthesis could reach up to 97 % yield compared to ~20 % of CNC while consuming less energy and chemicals [25,26]. AC synthesis is relatively simpler and more efficient than those of CNC and CNF [7,25]. AC is utilized as film [7], aerogel [25], and pellet [27]. In addition, the enhancement of AC properties by combining with other materials could diversify its usages.

Graphene oxide (GO) is a derivative of graphene with numerous functional groups such as epoxide, hydroxyl, and carboxyl on its surfaces and edges [28,29]. GO has unusual beneficial properties such as surface area (~2,630 m^2/g), mechanical flexibility, charge carrier mobility, hydrophilicity and dispersibility [9,30]. These unique properties make it an ideal additive for advanced composite materials.

Currently there are various cellulose-GO composites such as fiber [31], film [18,32], monolith [9], aerogel [33], layered membrane [34] and bead [10,35]. Among various composite forms, cellulose-GO bead composites are popularly employed in water purification, chromatography, and manufacturing industries [2]. The existing AC and amorphous cellulose-graphene oxide (ACGO) beads fabrication techniques are complicated, time and energy consuming. Thus, in this research we propose an efficient

methodology for AC and ACGO beads fabrication using less chemical under simple 2-step approach and we prepared AC and ACGO beads from H_2SO_4-gelatinized eucalyptus paper.

Materials and methods

Materials

Eucalyptus paper was purchased from phoenix pulp and paper PCL (Thailand). Analytical reagent grade of 97 wt% H_2SO_4 was purchased from Sigma-Aldrich and no purification was performed before usage. GO was synthesized via a modified Hummers method over oxidizing graphite with H_2SO_4 acid and $KMnO_4$ oxidizing agent, as previously reported by Phrompet *et al.* [36]. GO suspension in water with a concentration of 5 mg/mL was prepared. Water was further evaporated to obtained 10 wt% GO in water.

Preparation of AC and ACGO gels

Two sets of sulfuric acid solutions including 40 wt% H_2SO_4 (RT) and 65 wt% H_2SO_4 (pre-cooled to −20 °C) were employed for the preparation of AC and ACGO gel. Briefly, 1 g of eucalyptus paper was placed in a 25 mL beaker, then 4 mL of 40 wt% H_2SO_4 was poured into the beaker. The paper was immediately broken down into suspended fibers by a stirring rod. The process took approximately 1 min. Subsequently, 65 wt% H_2SO_4 was gradually added while mixing the suspension with a glass rod until the transparent cellulose gel was obtained. The H_2SO_4 gelatinization was performed in an ice bath. The process took approximately 6 min. A total of 4 mL of cold 65 wt% H_2SO_4 was employed for making the cellulose gel. To make a cellulose gel with graphene oxide, 2 mL of 10% GO in water was added into the gel and thoroughly mixed by a stirring rod for 1 min. Finally, 2 types of cellulose gel were obtained: Cellulose gel in cold sulfuric acid (AC gel), **Figure 1A**, and cellulose-GO gel in cold sulfuric acid (ACGO gel), **Figure 1B**.

Preparation of AC and ACGO beads

The ACGO gel was loaded into a 22-gauge syringe and droplet-extruded into a beaker containing 500 mL of deionized (DI) water. A white cellulose bead (AC bead) was immediately formed, as shown in **Figure 1A**. When the ACGO gel was droplet-extruded into DI water, an ACGO bead was generated as shown in **Figure 1B**. Finally, the beads were dialyzed against 1000 mL of DI water. DI water was replaced every 24 h until the pH reached that of DI water (pH = 5).

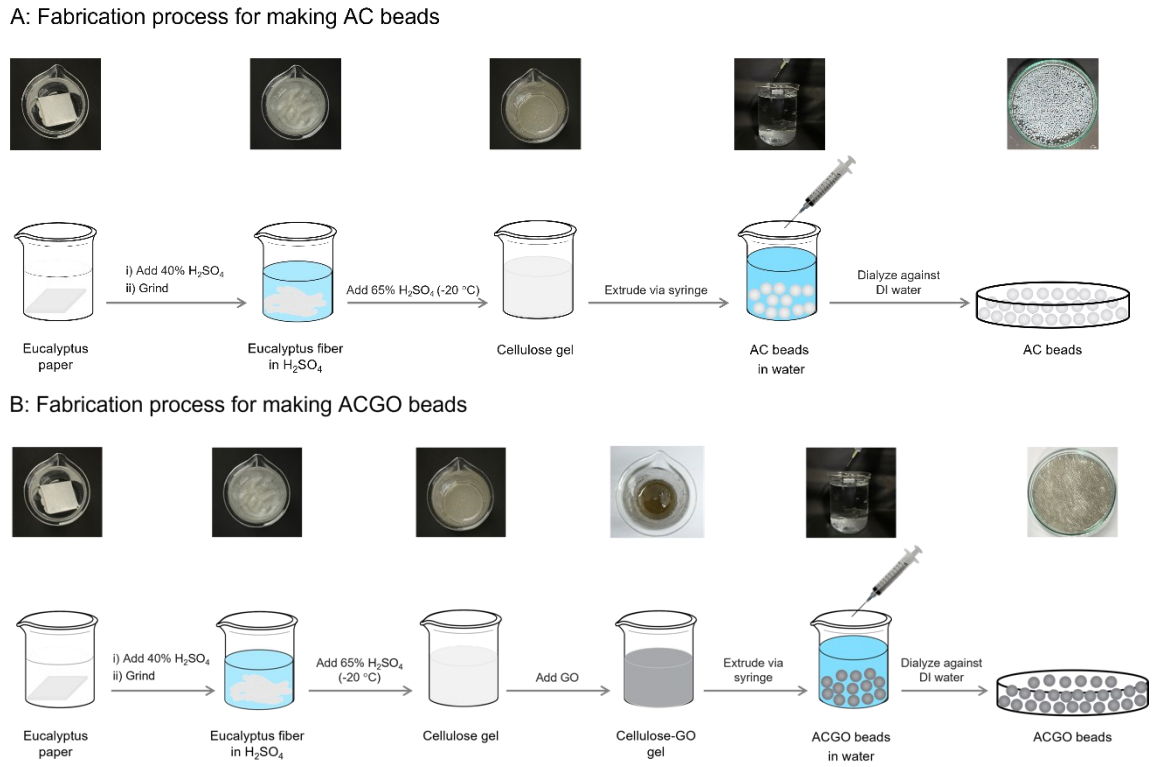

Figure 1 Fabrication process for making A) AC, and B) ACGO beads.

Characterization

The AC and ACGO beads were fixed onto a glass slide and then photographed. Size distribution of 200 beads were analyzed by Image J software (Image J bundled with Java 1.8.0_172, Bethesda, Maryland, USA). AC and ACGO beads were dried with vacuum drying prior to be analyzed by FTIR, Raman, TGA, XRD and SEM techniques. FTIR spectra were measured on a Nicolet iS5 FTIR spectrometer with iD7 ATR accessory (Thermo Fisher Scientific Inc., Waltham, Massachusetts, USA) in the range of 400 - 4000 cm^{-1} by averaging 32 co-addition scans at a resolution of 4 cm^{-1}. Raman spectra were recorded from 300 to 3000 cm^{-1} using a Raman microscope (Thermo Scientific DXR3 Raman microscope, Thermo Fisher Scientific Inc., Waltham, Massachusetts, USA) with a 532 nm excitation laser via a 100× objective lens. Thermal gravimetric analysis (TGA) was conducted by a thermogravimetric analyzer (PYRIS-1 TGA, Shelton, USA) in nitrogen atmosphere. The temperature program was 30 - 700 °C with 20 °C /min heating rate. X-ray diffraction (XRD) patterns were acquired using an X-Ray diffractometer (Bruker AXS Model D8 Discover, Billerica, Massachusetts, USA) operated at 40 kV and 40 mA with Cu K_α radiation. The diffraction angle was in range of 1 to 80 ° with a scanning speed of 2.5 °/min. The morphologies of eucalyptus paper, AC and ACGO bead were observed by a scanning electron microscope (JEOL - Model JSM-6510LV Series, Tokyo, Japan) with an accelerating voltage of 15 KV under high vacuum mode.

Results and discussion

The structural transformation of eucalyptus cellulose to AC and ACGO beads was shown in **Figures 2A** and **2B**, respectively. The cellulose chain is a polymer of β-D-glucopyranose unit connected via β-1,4 glycosidic bond. The cellulose chains assemble under a strong inter- and intra-molecular H-bonds into highly stable cellulose fiber with alternate crystalline and amorphous region [1,37].

The gelatinization and regeneration processes were employed for fabrication of AC and ACGO beads from non-soluble cellulose fibers. In detail, the 40 wt% H_2SO_4 aqueous solution unpacked the cellulose fibers into a small fragment making them easily gelled by the cold H_2SO_4, **Figure 1**. The addition of cold 65 wt% H_2SO_4 aqueous solution solvated and subsequently transformed the separated cellulose fibers to transparent viscose gel. A similar observation was reported by Huang *et al.* [7]. During the gelatinization process, 2 main reactions, H-bond breaking and esterification, occurred [7,27,38,39]. The H_2SO_4 disrupted the inter- and intra-molecular H-bonds making the cellulose chain separated. The 65 wt% H_2SO_4 aqueous solution pre-cooled to −20 °C was unable to break the β-1,4 glycosidic bonds because the cold temperature prevented the hydrolysis process [7,25]. After H-bonds were broken, the flexible cellulose chains could wrap around the GO plates. The OH groups on the cellulose chains could form H-bonding with the hydrophilic groups on the surface of GO sheet [34]. In the regeneration process, by droplet-extruded the gel into water, H_2SO_4 molecules were abstracted out of the gel. The re-formed H-bonding between cellulose chains turns the gel droplets into solid cellulose beads (**Figure 2A**), the cellulose gel with GO forms into ACGO beads as GO was trapped within the solid gel between the solidified cellulose chain (**Figure 2B**) as confirmed by the FTIR and Raman spectra.

The developed AC and ACGO bead fabrication technique was beneficial for making cellulose composite due to 3 main reasons. Firstly, the current methodology consumed less resources, energy, and time compared to the previously published methods [25,40]. Additionally, some solvent systems previously reported such as EMIMAc/DMSO [41], NMMO [42] and LiCl/DMAc systems [43] required high temperature for dissolution. Secondly, the H_2SO_4 acted as direct dissolution solvent for eucalyptus paper while NaOH/urea systems required partial hydrolysis of the material prior to dissolution process [23,37]. The dispersion of cellulose paper into small fragments (by an addition of 40 wt% H_2SO_4 aqueous solution) increased the gelatinization efficiency of the eucalyptus fiber by cold 65 wt% H_2SO_4, as shown in **Figure 1**. Thirdly, the cleaning process by dialysis of the beads was simpler compared to other systems such as NaOH/urea method [23,37]. Therefore, the main contribution to lower production cost in this study is due to the type of solvent used and the methodology of using 2 sets of sulfuric acid as solvent.

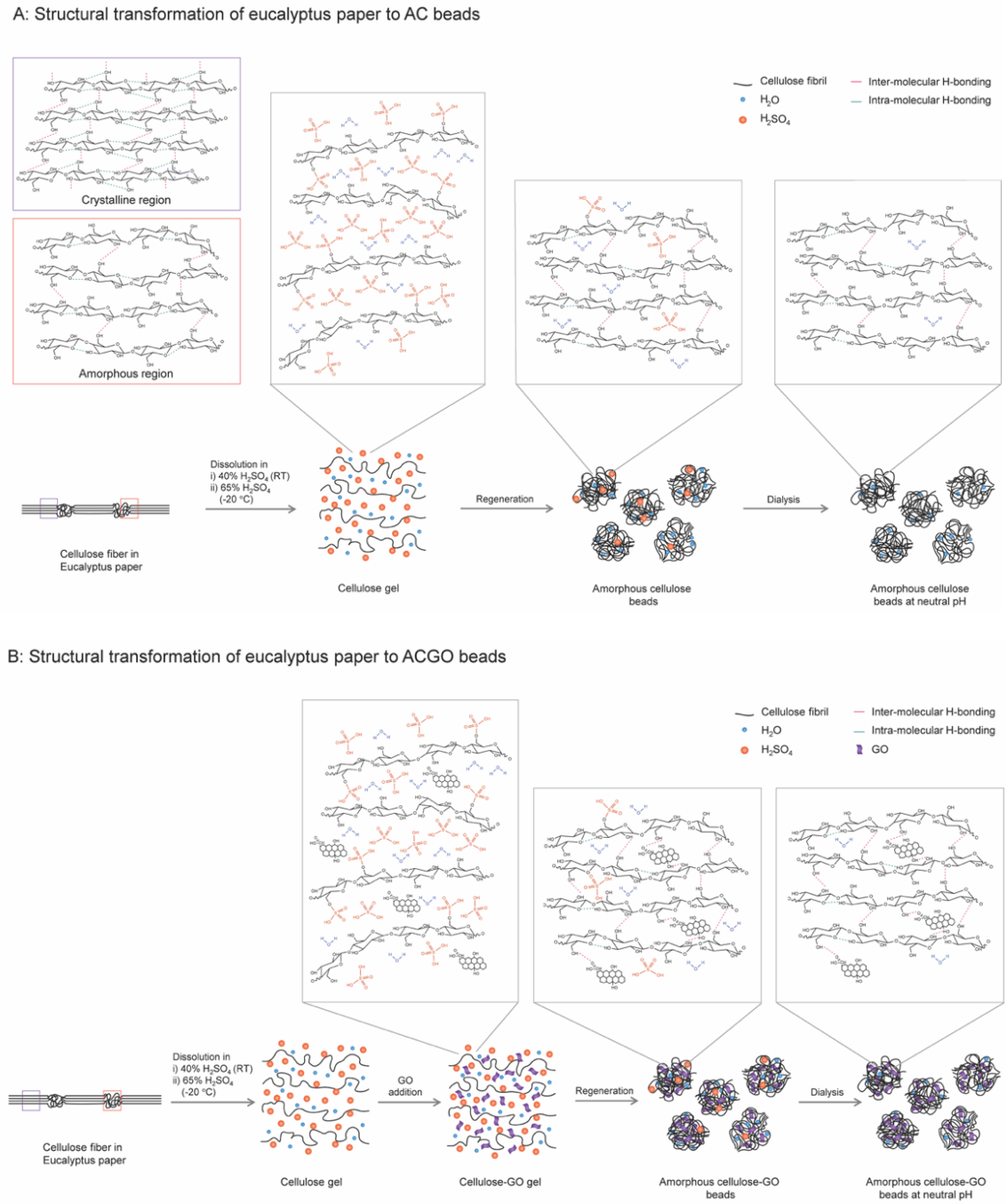

Figure 2 Schematic drawings show structural transformation of cellulose fiber in eucalyptus paper to A) AC, and B) ACGO beads.

The AC and ACGO beads were both quasi-sphere with AC beads having white (**Figure 3A**) while ACGO beads having light-brown colors (**Figure 3B**). The light-brown color of ACGO beads was due to the embedded GO in the regenerated amorphous cellulose. The histograms in **Figure 3** indicated that the AC beads had mean diameter (d_{AC}) of 2.11 ± 0.13 mm while that of ACGO beads (d_{ACGO}) were 2.14 ± 0.12 mm.

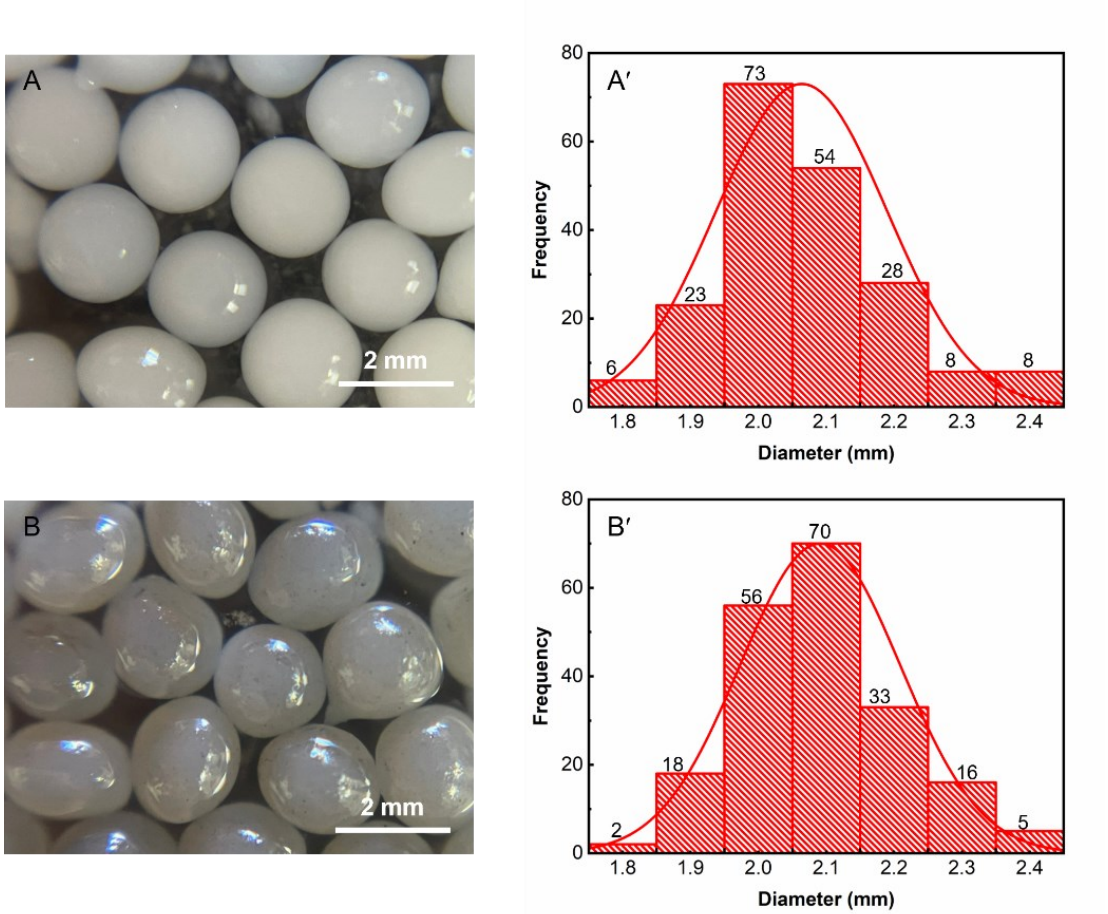

Figure 3 Photographic images of A) AC, and B) ACGO beads and their corresponding histograms.

Cellulose I and II were the most common celluloses in which cellulose I was in the native form while the cellulose II was in the swollen form after treatment of cellulose I [44]. The FTIR spectra of eucalyptus paper, AC, and ACGO beads were shown in **Figure 4A**. There was no new peak appeared after the eucalyptus paper was gelatinized and regenerated into AC and ACGO beads. However, there were 3 remarkable peak shifts confirming that cellulose I was successfully transformed to cellulose II after regeneration process. Firstly, the peaks at 3318 and 3314 cm^{-1} (OH stretching of intra-molecular H-bonding at O(3)H···O(5) in cellulose I) of eucalyptus paper shifted to 3327 cm^{-1} (OH stretching of intra-molecular H-bonding at O(3)H···O(5) of cellulose II). The OH stretching region became broader after the regeneration process. Secondly, the peak at 1430 cm^{-1} (CH_2 scissoring mode of C(6) in cellulose I) of eucalyptus paper decreased in intensity and shifted to 1424 cm^{-1} (CH_2 scissoring mode of C(6) in cellulose II). This shift indicated the disappearance of crystalline structure of cellulose I as its transformed to the amorphous structure of cellulose II. Lastly, the peak intensity at 899 cm^{-1} (C-O-C stretching symmetric of glycosidic linkage of cellulose II) increased. These spectroscopic changes, which directly associated with molecular structures, confirmed that the inter- and intra-molecular H-bonds in cellulose I structure had disappeared and new arrangement of disordered H-bonding in cellulose II had formed [7,37,45,46]. Although FTIR spectra did not show characteristic peaks of GO in ACGO bead but Raman spectra clearly revealed characteristic peaks of GO (**Figure 4B**). Two strong peaks at 1350 and 1590 cm^{-1} of the ACGO curve were assigned as D and G bands, respectively [47]. The intensity ratio (I_D/I_G) of 1.3 indicated abundance of oxygen-containing functional groups on GO which promoting its interaction with OH groups in amorphous cellulose (as depicted in **Figure 2B**). The observed spectroscopic information confirmed that GO was successfully embedded in amorphous cellulose structure.

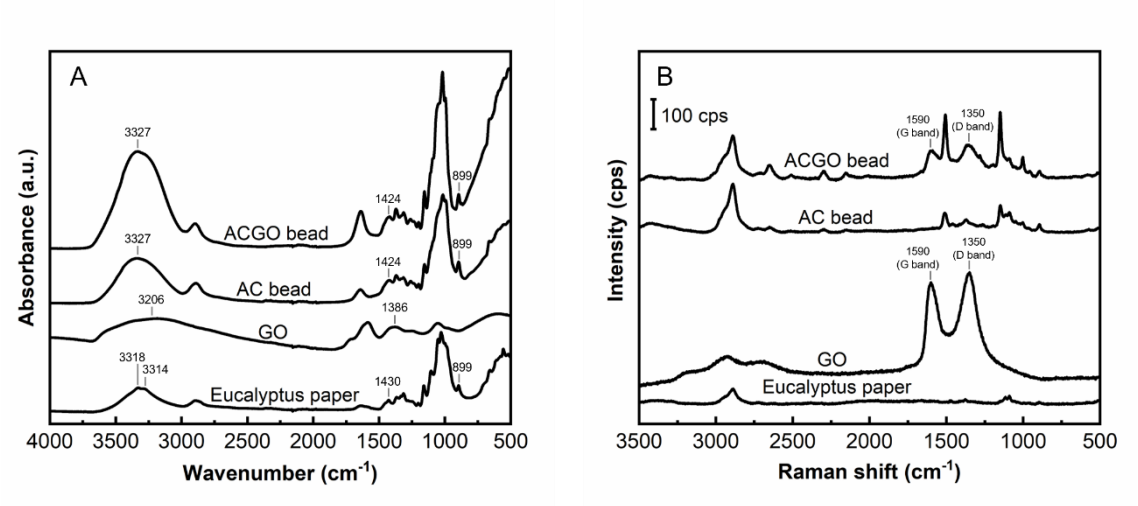

Figure 4 A) FTIR and B) Raman spectra of eucalyptus paper, GO, AC and ACGO beads.

The thermal activities of eucalyptus paper, AC and ACGO beads were studied by thermal gravimetric analysis (TGA, **Figure 5A**) and derivative weight loss analysis (DTG, **Figure 5B**). All samples showed small weight loss below 100 °C due to evaporation of water [48]. At 200 to 400 °C, the decomposition of all samples was attributed to the depolymerization and decomposition of cellulose [49]. The thermal degradation of eucalyptus paper started at the onset temperature (T_{onset}) of 300 °C and reached peak temperature (T_{peak}) at 380 °C. Both the AC and ACGO beads were less thermally stable than the eucalyptus paper with an approximate T_{onset} of 200 °C since they had higher portion of amorphous cellulose [48]. In addition, the small peak at 500 °C was attributed to trace lignin decomposition [50]. A 20 % char yield of ACGO beads at 700 °C was attributed to the residual GO as it decomposes at a higher temperature (~850 °C) [33].

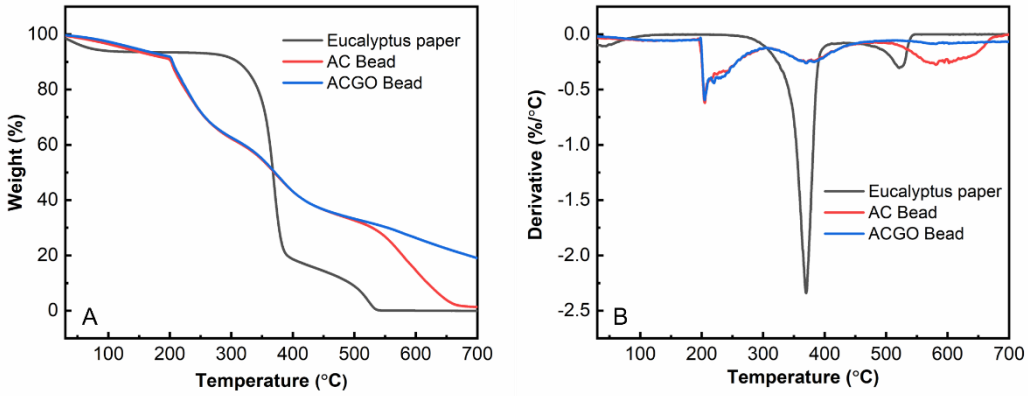

Figure 5 (A) TGA and (B) DTG curves of eucalyptus paper, AC and ACGO beads.

XRD patterns of eucalyptus paper, AC, and ACGO beads were shown in **Figure 6**. The patterns confirmed the transformation of cellulose I to cellulose II up on gelatinization and subsequent regeneration of the semicrystalline eucalyptus paper. The XRD pattern of eucalyptus paper showed typical diffraction peaks at 17.1 and 22.7 ° corresponding to cellulose I [51-53]. The crystallinity index (CI) of 83 %, calculated from the XRD pattern in **Figure 6** using Segal formular [53], suggested that the employed eucalyptus fiber was a semicrystalline cellulose with high portion of cellulose I.

XRD patterns of AC and ACGO beads in **Figure 6**, however, did not show any diffraction signature of semicrystalline cellulose at 17.1 or 22.7 °. The XRD patterns of AC and ACGO bead, on the other hand, showed a single broad peak at 21.9 °, attributing to cellulose II or amorphous cellulose [7]. Our observation is similar to those report by Park *et al.* [54]. The CI% of AC and ACGO bead could not be calculated due to a completed transformation of semicrystalline cellulose to amorphous cellulose under the gelatinization and regeneration process.

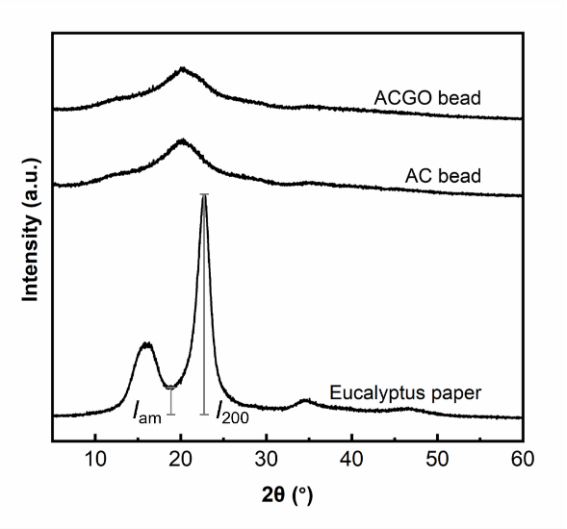

Figure 6 XRD patterns for eucalyptus paper, AC and ACGO beads.

SEM images of eucalyptus paper, AC and ACGO beads were shown in **Figure 7**. **Figure 7A** illustrated that the eucalyptus paper consisted of fibers with diameters of 10 - 15 μm. The SEM image of AC beads (after drying, **Figure 7B**) revealed a rough surface while that of ACGO beads revealed a smoother surface (**Figure 7C**). The interaction of the added GO with the OH groups in amorphous cellulose may result in a smoother surface of ACGO beads as the surface of GO is abundant in hydrophilic groups [36, 51,52,55]. ACGO composites were applicable in products such as adsorbent [33,34], film [7], and bead [40]. It indicates that ACGO composites have potential to be in industries such as films and water treatment.

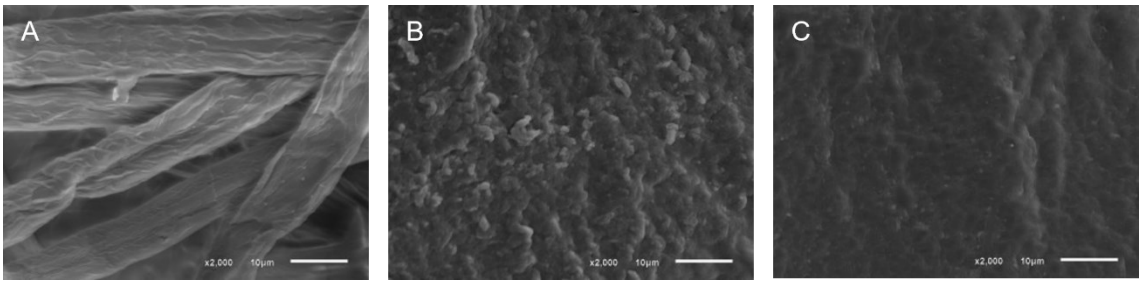

Figure 7 SEM images of A) eucalyptus paper, B) AC, and C) ACGO beads.

Conclusions

A simple and effective methodology for fabricating uniform AC and ACGO beads was successfully developed. The average sizes of AC and ACGO beads had average diameter of 2.11 ± 0.13 and 2.14 ± 0.12 mm, respectively. The structural change of semicrystalline eucalyptus fiber after gelatinization and subsequent regeneration were investigated using molecular, thermal, and structural characterization techniques. FTIR spectra and XRD patterns confirmed the transformation of cellulose I to cellulose II. Raman spectra confirmed the embedding of GO within amorphous cellulose chains in ACGO beads. The SEM images revealed a smoother surface of ACGO beads compared to that of the AC beads because of the added GO. The hydrophilic groups on the surface of the GO could efficiently interact with the hydroxyl groups of amorphous cellulose.

Acknowledgements

This research was supported by Ratchadapisek Somphot Fund (Chulalongkorn University) and the Research Network NANOTEC (RNN) program of the National Nanotechnology Center (NANOTEC), NSTDA, Ministry of Higher Education, Science, Research and Innovation, Thailand.

References

[1] L Jasmani and W Thielemans. Preparation of nanocellulose and its potential application. *Forest Res*. 2018; **7**, 1000222.

[2] K Tan, S Heo, M Foo, I M Chew and C Yoo. An insight into nanocellulose as soft condensed matter: Challenge and future prospective toward environmental sustainability. *Sci. Total Environ*. 2019; **650**, 1309-26.

[3] N Soykeabkaew, N Tawichai, C Thanomsilp and O Suwantong. Nanocellulose-reinforced "green" composite materials. *Walailak J. Sci. Tech*. 2016; **14**, 353-68.

[4] C Mhumak and C Pechyen. Development and characterization of polypropylene/polyethylene vinyl acetate/micro cellulose trays as a prototype for chilled food packaging application. *Walailak J. Sci. Tech*. 2018; **15**, 765-77.

[5] M A Herrera, A P Mathew and K Oksman. Barrier and mechanical properties of plasticized and cross-linked nanocellulose coatings for paper packaging applications. *Cellulose* 2017; **24**, 3969-80.

[6] Y Zhou, S Sun, W Bei, MR Zahi, Q Yuan and H Liang. Preparation and antimicrobial activity of oregano essential oil pickering emulsion stabilized by cellulose nanocrystals. *Int. J. Biol. Macromol*. 2018; **112**, 7-13.

[7] W Huang, Y Wang, L Zhang and L Chen. Rapid dissolution of spruce cellulose in H_2SO_4 aqueous solution at low temperature. *Cellulose* 2016; **23**, 3463-73.

[8] Y Tang, X Zhang, R Zhao, D Guo and J Zhang. Preparation and properties of chitosan/guar gum/nanocrystalline cellulose nanocomposite films. *Carbohydr. Polym*. 2018; **197**, 128-36.

[9] A Hussain, J Li, J Wang, F Xue, Y Chen, TB Aftab and D Li. Hybrid monolith of graphene/TEMPO-oxidized cellulose nanofiber as mechanically robust, highly functional, and recyclable adsorbent of methylene blue dye. *J. Nanomater*. 2018; **3**, 1-12.

[10] N Mohammed, N Grishkewich, RM Berry and KC Tam. Cellulose nanocrystal-alginate hydrogel beads as novel adsorbents for organic dyes in aqueous solutions. *Cellulose* 2015; **22**, 3725-38.

[11] J Erlandsson, V López Durán, H Granberg, M Sandberg, PA Larsson and L Wågberg. Macro- and mesoporous nanocellulose beads for use in energy storage devices. *Appl. Mater. Today* 2016; **5**, 246-54.

[12] K Yuwawech, J Wootthikanokkhan, S Wanwong and S Tanpichai. Polyurethane/esterified cellulose nanocrystal composites as a transparent moisture barrier coating for encapsulation of dye sensitized solar cells. *J. Appl. Polym. Sci*. 2017; **134**, 45010.

[13] DG Gray. Recent advances in chiral nematic structure and iridescent color of cellulose nanocrystal films. *J. Nanomater.* 2016; **6**, 213.

[14] JPF Lagerwall, C Schütz, M Salajkova, J Noh, J Hyun Park, G Scalia and L Bergström. Cellulose nanocrystal-based materials: From liquid crystal self-assembly and glass formation to multifunctional thin films. *NPG Asia Mater*. 2014; **6**, e80.

[15] S Cao, P Xu, Y Ma, X Yao, Y Yao, M Zong, X Li and W Lou. Recent advances in immobilized enzymes on nanocarriers. *Chinese J. Catal*. 2016; **37**, 1814-23.

[16] Y Li, S Yu, P Chen, R Rojas, A Hajian and L Berglund. Cellulose nanofibers enable paraffin encapsulation and the formation of stable thermal regulation nanocomposites. *Nano Energ.* 2017; **34**, 541-8.

[17] LE Millon and WK Wan. The polyvinyl alcohol-bacterial cellulose system as a new nanocomposite for biomedical applications. *J. Biomed. Mater. Res. B Appl. Biomater*. 2006; **79**, 245-53.

[18] D Trache, AF Tarchoun, M Derradji, TS Hamidon, N Masruchin, N Brosse and MH Hussin. Nanocellulose: From fundamentals to advanced applications. *Front. Chem*. 2020; **8**, 392.

[19] D Trache, MH Hussin, MK Haafiz and VK Thakur. Recent progress in cellulose nanocrystals: Sources and production. *Nanoscale* 2017; **9**, 1763-86.

[20] M Iqhrammullah, M and S Nur. Adsorption behaviour of hazardous dye (methyl orange) on cellulose-acetate polyurethane sheets. *Mater. Sci. Eng*. 2020; **845**, 012035.

[21] M Iqhrammullah, H Suyanto, Rahmi, M Pardede, I Karnadi, KH Kurniawan, W Chiari and SN Abdulmadjid. Cellulose acetate-polyurethane film adsorbent with analyte enrichment for in-situ dectection and analysis of aqueous Pb using laser-induced breakdown spectroscopy (LIBS). *Environ. Nanotechnol. Monit. Manag.* 2021; **16**, 100516.

[22] S Alila, I Besbes, MR Vilar, P Mutjé and S Boufi. Non-woody plants as raw materials for production of microfibrillated cellulose (MFC): A comparative study. *Ind. Crops Prod*. 2013; **41**, 250-9.

[23] X Gong, Y Wang, Z Tian, X Zheng and L Chen. Controlled production of spruce cellulose gels using an environmentally "green" system. *Cellulose* 2014; **21**, 1667-78.

[24] M Jonoobi, R Oladi, Y Davoudpour, K Oksman, A Dufresne, Y Hamzeh and R Davoodi. Different preparation methods and properties of nanostructured cellulose from various naporal resources and residues: A review. *Cellulose* 2015; **22**, 935-69.
[25] R Hashaikeh and H Abushammala. Acid mediated networked cellulose: Preparation and characterization. *Carbohydr. Polym*. 2011; **83**, 1088-94.
[26] D Bondeson, A Mathew and K Oksman. Optimization of the isolation of nanocrystals from microcrystalline cellulose by acid hydrolysis. *Cellulose* 2006; **13**, 171-80.
[27] YHP Zhang, J Cui, LR Lynd and LR Kuang. A transition from cellulose swelling to cellulose dissolution by o-phosphoric acid: Evidence from enzymatic hydrolysis and supramolecular structure. *Biomacromolecules* 2006; **7**, 644-8.
[28] TS Vo, T Vo, JW Suk and K Kim. Recycling performance of graphene oxide-chitosan hybrid hydrogels for removal of cationic and anionic dyes. *Nano Converg*. 2020; **7**, 4.
[29] X Wang, G Peng, M Chen, M Zhao, Y He, Y Jiang, X Zhang, Y Qin and S Lin. Reduced graphene oxide composites and its real-life application potential for in-situ crude oil removal. *Chemosphere* 2020; **249**, 126141.
[30] P Shandilya, A Sudhaik, P Raizada, A Hosseini-Bandegharaei, P Singh, A Rahmani-Sani, V Thakur and A K Saini. Synthesis of Eu^{3+-} doped ZnO/Bi_2O_3 heterojunction photocatalyst on graphene oxide sheets for visible light-assisted degradation of 2,4-dimethyl phenol and bacteria killing. *Solid State Sci*. 2020; **102,** 106164.
[31] L Chen, Y Li, S Hu, J Sun, Q Du, X Yang, Q Ji, Z Wang, D Wang and Y Xia. Removal of methylene blue from water by cellulose/graphene oxide fibres. *J. Exper. Nanosci*. 2016; **11**, 1156-70.
[32] K Tu, Q Wang, A Lu and L Zhang. Portable visible-light photocatalysts constructed from Cu_2O nanoparticles and graphene oxide in cellulose matrix. *J. Phys. Chem. C*. 2014; **118**, 7202-10.
[33] F Ren, Z Li, WZ Tan, XH Liu, ZF Sun, PG Ren and DX Yan. Facile preparation of 3D regenerated cellulose/graphene oxide composite aerogel with high-efficiency adsorption towards methylene blue. *J. Colloid Interface Sci*. 2018; **532**, 58-67.
[34] Y Qiufang, F Bitao, X Ye, J Chunde, S Qingfeng and S Chengmin. 3D assembly based on 2D structure of cellulose nanofibril/ graphene oxide hybrid aerogel for adsorptive removal of antibiotics in water. *Sci*. 2017; **7**, 45914.
[35] L Zhao, S Yang, A Yilihamu, Q Ma, M Shi, B Ouyang, Q Zhang, X Guan and ST Yang. Adsorptive decontamination of Cu^{2+}contaminated water and soil by carboxylated graphene oxide/chitosan/cellulose composite beads. *Environ. Res*. 2019; **179**, 108779.
[36] C Phrompet, C Sriwong and C Ruttanapun. Mechanical, dielectric, thermal and antibacterial properties of reduced graphene oxide (rGO)-nanosized C3AH6 cement nanocomposites for smart cement-based materials. *Compos. B* 2019; **175**, 107128.
[37] R Li, S Wang, A Lu and L Zhang. Dissolution of cellulose from different sources in an NaOH/urea aqueous system at low temperature. *Cellulose* 2015; **22**, 339-49.
[38] Y Wang, X Wang, Y Xie and K Zhang. Functional nanomaterials through esterification of cellulose: A review of chemistry and application. *Cellulose* 2018; **25**, 3703-31.
[39] Z Junhua, Z Jingqiang, L Lu, C Tianming, Z Jun, L Shijie, L Zhenjiang and O Pingkai. Dissolution of microcrystalline cellulose in phosphoric acid molecular changes and kinetics. *Molecules* 2009; **14**, 5027-41.
[40] X Zhang, H Yu, H Yang, Y Wan, H Hu, Z Zhai and J Qin. Graphene oxide caged in cellulose microbeads for removal of malachite green dye from aqueous solution. *J. Colloid Interface Sci*. 2015; **437**, 277-82.
[41] R Lu, X Zhang, L Fu, H Wang, R M Briber and H Wang. Amorphous cellulose thin films. *Cellulose* 2020; **27**, 2959-65.
[42] M Michael, RN Ibbett and OW Howarth. Interaction of cellulose with amine oxide solvents. *Cellulose* 2000; **7**, 21-33.
[43] CL McCormick, PA Callais and BH Hutchinson Jr. Solution studies of cellulose in lithium chloride and N,AT-Dimethylacetamide. *Macromolecules* 1985; **18**, 2394-401.
[44] SP Gautam, PS Bundela, AK Pandey, Jamaluddin, MK Awasthi and S Sarsaiya. A review of systematic study of cellulose. *J. Nat. Appl. Sci*. 2010; **2**, 330-43.
[45] F Carrillo, X Colom, JJ Suñol and J Saurina. Structural FTIR analysis and thermal characterisation of lyocell and viscose-type fibres. *Eur. Polym. J*. 2004; **40**, 2229-34.
[46] H Yu, Z Qin, B Liang, N Liu, Z Zhou and L Chen. Facile extraction of thermally stable cellulose nanocrystals with a high yield of 93 % through hydrochloric acid hydrolysis under hydrothermal conditions. *J. Mater. Chem. A* 2013; **1**, 3938-44.

[47] S Stankovich, DA Dikin, RD Piner, KA Kohlhaas, A Kleinhammes, Y Jia, Y Wu, ST Nguyen and RS Ruoff. Synthesis of graphene-based nanosheets via chemical reduction of exfoliated graphite oxide. *Carbon* 2007; **45**, 1558-65.

[48] X Tan, L Chen, X Li and F Xie. Effect of anti-solvents on the characteristics of regenerated cellulose from 1-ethyl-3-methylimidazolium acetate ionic liquid. *Int. J. Biol. Macromol* 2019; **124**, 314-20.

[49] MR and WT Winter. Effect of sulfate groups from sulfuric acid hydrolysis on the thermal degradation behavior of bacterial cellulose. *Biomacromolecules* 2004; **5**, 1671-7.

[50] MVF Ferreira, ACC Neves, CGD Oliveira, FPD Lopes, FM Margem, CMF Vieira and SN Monteiro. Thermogravimetric characterization of polyester matrix composites reinforced with eucalyptus fibers. *J. Mater. Res. Tech*. 2017; **6**, 396-400.

[51] E Leng, Y Zhang, Y Peng, X Gong, M Mao, X Li and Y Yu. In situ structural changes of crystalline and amorphous cellulose during slow pyrolysis at low temperatures. *Fuel* 2018; **216**, 313-21.

[52] K Hattori and A Arai. Preparation and hydrolysis of water-stable amorphous cellulose. *ACS Sustain. Chem. Eng*. 2016; **4**, 1180-6.

[53] L Segal, JJ Creely, AE Martin Jr and CM Conrad. An empirical method for estimating the degree of crystallinity of native cellulose using the X-Ray diffractometer. *Text. Res. J*. 1959; **29**, 786-94.

[54] S Park, JO Baker, ME Himmel, PA Parilla and DK Johnson. Cellulose crystallinity index: Measurement techniques and their impact on interpreting cellulase performance. *Biotechnol. Biofuels* 2010; **3**, 10.

[55] Rahmi, S Lubis, N A Zahra, K Puspita and M Iqhrammullah. Synergetic photocatalytic and adsorptive removals of metanil yellow using TiO_2/Grass-derived cellulose/chitosan film composite. *Int. J. Eng.* 2021; **34,** 1827-36.